Ultrahigh-density superhard hexagonal BN and SiC with quartz topology from crystal chemistry and first principles

Samir Matar, Vladimir Solozhenko

Ultrahigh-density superhard hexagonal BN and SiC with quartz topology from crystal chemistry and first principles

Samir F. Matar[1] and Vladimir L. Solozhenko[2,*]

[1] Lebanese German University, Jounieh, P.O. Box 206, Lebanon
https://orcid.org/0000-0001-5419-358X

[2] LSPM–CNRS, Université Sorbonne Paris Nord, 93430 Villetaneuse, France
https://orcid.org/0000-0002-0881-9761

Abstract

*Based on superdense C_6 with quartz (**qtz**) topology, new ultrahigh-density hexagonal binary phases, **qtz** BN and **qtz** SiC, have been identified from full geometry structure relaxations and ground state energies using calculations based on the quantum density functional theory (DFT) with gradient GGA exchange-correlation XC functional. Like **qtz** C_6 with respect to diamond, the resulting binary **qtz** BN and **qtz** SiC were found to be less cohesive than cubic BN and cubic SiC, respectively, but were confirmed to be mechanically (elastic constants) and dynamically (phonon band structures) stable. Higher densities of the new phases correlate with their higher hardness values compared to cubic BN and cubic SiC. In contrast to the regular tetrahedra that characterize the cubic BN and SiC phases, the corner-sharing tetrahedra in the new phases are distorted, which accounts for their exceptional density and hardness. All three **qtz** phases were found to be semiconducting to insulators with reduced band gaps compared to diamond, cubic BN and cubic SiC.*

Keywords: BN; SiC; DFT; topology; hardness; phonons; thermodynamics; band structures

* Corresponding author (e-mail: vladimir.solozhenko@univ-paris13.fr)

Introduction

Diamond is the hardest known material with a Vickers hardness (H_V) at the level of 100 GPa and density ρ = 3.635 g/cm^3 [1]. Its structure (space group *Fm*-3*m*) is formed by corner-sharing tetrahedra of sp^3-hybridized carbon atoms with ∠C-C-C = 109.47° and is characterized by the highest atomic density (i.e., the number of atoms per unit cell volume) and the highest density per valence electron [2]. A rare hexagonal form of diamond (lonsdaleite) (space group $P6_3/mmc$) with virtually the same density has been claimed to be stronger and stiffer than diamond [3].

The network topologies of diamond and lonsdaleite are **dia** and **lon**, respectively, and many theoretically predicted carbon allotropes have been identified with these topologies (see [4] and references therein). The topology determination for the new phases is now made easy with the TopCryst program [5]. Information on all carbon allotropes extracted from the literature is indexed in the "SACADA" database [6], which currently contains 703 allotropes.

Diamond (both cubic and hexagonal) is still considered to have superior atomic density, elastic moduli and hardness [1]. Recently, however, several superdense (ρ > 3.635 g/cm^3) carbon allotropes have been predicted from the first-principles studies [7,8], and hexagonal (space group P_6222) C_3 with assigned quartz topology (SACADA **qtz** #11) has even been claimed to have a hardness of 113 GPa [8], i.e., 15% harder than diamond. Also, very recently superdense (ρ = 3.666 g/cm^3) ultrahard ($H_V \approx$ 102 GPa) hexagonal C_6 (space group $P6_522$) allotrope with **qtz** topology was proposed by us [9].

The quartz topology is also observed in binary (ZnTe) and ternary ($GaAsO_4$, $FePO_4$) compounds. In particular, under pressure, in addition to the cubic sphalerite structure (space group *F*-43*m*) characteristic of zinc chalcogenides, ZnTe also exhibits a trigonal α-HgS-type structure (space group $P3_121$) [10] with **qtz** topology. This may be because the Pauling electronegativity (χ)of the chalcogen decreases from oxygen (χ(O) = 3.44) to tellurium (χ(Te) = 2.10). Knowing χ(Zn) = 1.65, ZnO is an ionic compound ($\Delta\chi$|Zn-O|=1.79), while ZnTe is already a covalent compound ($\Delta\chi$|Zn-Te| = 0.45).

In this regard, the aim of the present work was to search for ultrahigh-density superhard polymorphs of the binary compounds BN and SiC with quartz topology based on **qtz** C_6 [9] by quantum mechanical calculations of crystal structures and physical properties in the framework of Density Functional Theory (DFT) [11,12].

Computational framework

The structures of the binary compounds have all been subjected to geometry relaxations of the atomic positions and lattice constants down to the respective ground states characterized by minimum energies. The protocol consists of iterative calculations performed using the DFT-based plane-wave Vienna Ab initio Simulation Package (VASP) [13,14]. For the atomic potentials, the projector augmented wave (PAW) method was used [14,15]. The exchange and correlation effects were treated within a Generalized Gradient Approximation (GGA) scheme [16]. The relaxation of the atoms to the ground state geometry was done by applying a conjugate-gradient algorithm [17]. A tetrahedron method [18] with corrections according to the Methfessel-Paxton scheme [19] was used for geometry

optimization and energy calculations, respectively. A special *k*-point sampling [20] was applied to approximate the reciprocal space Brillouin zone (BZ) integrals. For better reliability, the optimization of the structural parameters was carried out along with successive self-consistent cycles with increasing k-mesh until the forces on atoms were less than 0.02 eV/Å and the stress components were below 0.003 eV/Å^3. The plane waves energy cutoff was 400 eV.

The mechanical properties were derived from the elastic constants calculations [21,22]. The phonon dispersion band structures were calculated to verify the dynamic stability of the new phases. The phonon modes were computed considering the harmonic approximation by finite displacements of the atoms around their equilibrium positions to obtain the forces from the summation over the different configurations. The phonon dispersion curves along the direction of the Brillouin zone were then obtained using the "Phonopy" interface code [23]. The crystal information files (CIF), the structure sketches including the tetrahedral representations as well as the illustrations of the charge density plots were generated using the VESTA graphics software [24]. The electronic band structures and densities of states were obtained with the full-potential augmented spherical wave ASW method based on DFT using the same GGA scheme as above [25].

Crystal chemistry

The structure of **qtz** C_6 is shown in Fig. 1a. A differentiation of carbon into two different sites was highlighted by resolving the initial C_6 structure (space group $P6_522$, No. 179) with unique (6a) sites [9] into carbon atoms with (3c) and (3d) Wyckoff positions within space group $P6_422$, No. 181 as shown in Table 1. Such an elementary modification allowed to consider the binary compounds B_3N_3 and Si_3C_3. The lattice parameters of the ground state structures are given in columns 3 to 5 of Table 1. The corresponding crystal structures are shown in Figs. 1b – 1d with ball-and-stick and tetrahedral representations, the latter being characterized by corner sharing irregular tetrahedra (*vide infra*). The atoms are described with general Wyckoff positions, i.e., at (3c) ½, 0, 0 and at (3d) ½, 0, ½. Differences are observed in the volumes (total and atom-averaged) and in the interatomic distances, which increase along the series due to the increase in the respective atomic radii. If we look at the angles related to the constituent tetrahedra, they differ significantly from the regular tetrahedral one (∠109.47°), thus indicating the specificity of the **qtz** topology.

All three **qtz** phases were found to be cohesive with negative E_{coh}/atom values (see Table 1), which are systematically lower than the corresponding values of diamond (-2.43 eV), cubic BN (-2.63 eV) and cubic SiC (-1.72 eV).

Mechanical properties from the elastic constants

The analysis of the mechanical behavior was carried out using the elastic properties by performing finite distortions of the lattice. The phase is then described by the bulk (*B*) and the shear (*G*) moduli obtained by averaging of the elastic constants. Here we used Voigt's method (cf. original [21] and modern [22] works) based on a uniform strain. The calculated sets of elastic constants C_{ij} (i and j

corresponding to directions) are given in Table 2. All C_{ij} values are positive. The elastic constants of **qtz** C_6 have the largest values, close to diamond [1], and smaller magnitudes were obtained for **qtz** BN and **qtz** SiC. The bulk (B_V) and shear (G_V) moduli (see the last two columns of Table 2) were calculated using the equations for the hexagonal system [22]:

$$B_V = 1/9\ \{2(C_{11} + C_{12}) + 4C_{13} + C_{33}\}$$

$$G_V = 1/30\ \{C_{11} + C_{12} + 2C_{33} - 4C_{13} + 12C_{44} + 12C_{66}\}$$

qtz C_6 has the largest moduli, close to the accepted values for diamond (B_V =445 GPa and G_V = 550 GPa [1]), while the binary phases, especially **qtz** SiC, have much smaller values.

Four modern theoretical models [26-29] have been used to predict the Vickers hardness (H_V) of new phases. The thermodynamic (T) model [26], which is based on thermodynamic properties and crystal structure, generally shows good agreement with experiment, and is therefore recommended for hardness evaluation of superhard and ultrahard phases [30]. The Vickers hardness and bulk modulus values calculated using this model are summarized in Table 3. The Lyakhov-Oganov (LO) model [27] takes into account the topology of the crystal structure, the strength of covalent bonding, the degree of ionicity and directionality; and the empirical models, Mazhnik-Oganov (MO) [28] and Chen-Niu (CN) [29], are based on elastic properties, namely, bulk and shear moduli. As shown previously [30], in the case of superhard ($H_V \geq 40$ GPa) compounds of light elements, the Lyakhov-Oganov model gives slightly underestimated values of hardness, while empirical models are not reliable. Fracture toughness (K_{Ic}) was evaluated using the Mazhnik-Oganov model [28]. Table 4 shows the hardness and other mechanical properties of the dense carbon, BN and SiC phases calculated using all four models.

It is noteworthy that the density of all three phases with quartz topology is higher than the density of the corresponding cubic phases (see Table 3), i.e., **qtz** C_6, **qtz** BN and **qtz** SiC are ultrahigh density phases.

The hardness and mechanical properties of **qtz** C_6 are, as expected, close to those of diamond and lonsdaleite. The corresponding values for **qtz** BN and especially for **qtz** SiC are significantly lower and are at the level of the mechanical properties of cubic boron nitride and cubic silicon carbide, respectively. It should be noted, however, that the hardness of all three phases with quartz topology is about 5% higher than that of the corresponding cubic phases. Such increased hardness is probably related to the ultrahigh densities of the **qtz** phases resulting from the distorted tetrahedron building blocks.

Dynamic and thermal properties from the phonons

Phonon band structures

A relevant criterion for phase stability can be obtained from the dynamic properties derived from the phonon modes. The phonon energies for **qtz** C_6, **qtz** BN and **qtz** SiC were then calculated, and the corresponding band structures were plotted along the hexagonal Brillouin zone in the reciprocal space. The corresponding band structures are shown in Fig. 2.

The bands develop along the main lines (horizontal direction) of the hexagonal Brillouin zone (reciprocal k-space). The vertical direction shows the frequencies ω, which are given in terahertz (THz). There are 3N phonon total modes with 3 acoustic modes starting from zero frequency (ω = 0 at the Γ point, center of the Brillouin zone), up to a few terahertz and 3N-3 optical modes at frequencies higher than three. The three acoustic modes correspond to the lattice rigid translation modes with two transverse modes and one longitudinal mode. The remaining bands correspond to the optical modes. In all three subfigures there are no negative frequencies, and the corresponding carbon allotrope and two binary phases are dynamically stable. The latter indicates that these phases, once synthesized, can exist at ambient conditions. In **qtz** C_6, the highest band culminates in the vicinity of ω ~ 40 THz, a value that has been observed for diamond by Raman spectroscopy [39]. Binary compounds are characterized by lower energy bands. ....

Thermodynamic properties

The thermodynamic properties of the new phases were calculated from the phonon frequencies using the statistical thermodynamic approach [40] on a high-precision sampling mesh in the Brillouin zone. The temperature dependencies of the heat capacity at constant volume (C_v) and entropy (S) of **qtz** C_6, **qtz** BN and **qtz** SiC are shown in Fig. 3 in comparison with experimental C_v data for diamond [41,42], cubic BN [43] and cubic SiC [44]. It is quite expected that the heat capacities of all three phases with quartz topology formed by distorted tetrahedra are higher than the heat capacities of the corresponding cubic phases.

Electronic band structures and density of states

Using the crystal structure parameters given in Table 1, the electronic band structures were obtained using the all-electrons DFT-based augmented spherical method (ASW) [25] and are shown in Figure 4. The bands develop along the main directions of the primitive hexagonal Brillouin zones. To the extent that all three phases exhibit band structures characterized by energy gaps between the valence band (VB) and the empty conduction band (CB), the energy reference along the vertical energy axis is with respect to the top of the VB: ($E-E_V$). **qtz** C_6 has a twice smaller band gap than diamond (~5 eV), showing a different behavior between **dia** and **qtz** topologies in the electronic structure behavior. The largest band gap is observed for **qtz** BN, which remains smaller than for cubic BN. The same feature of reduced band gap is observed for **qtz** SiC. It is also relevant to highlight that continuous VB in **qtz** C_6 versus two blocks in the binary compounds with a separation between low energy lying s-like states and higher energy lying p-like states up to E_V. In conclusion, the phases with **qtz** topology are provided with enhanced covalence.

The band structure features are reflected in the site-projected electronic densities of states, DOS, shown in Fig. 5 with energy along the horizontal axis and DOS in 1/eV units along the vertical axis. **qtz** C_6, expressed as $C1_3C2_3$, is characterized by identical DOS for both sites and a continuous VB extending over ~27 eV, indicating the purely covalent nature of the carbon allotrope. The sharp DOS

peak at 1 eV below EV belongs to the carbon p-states, which are more localized than the s-states smeared in the lower part of the VB. The (empty) CB also shows structured p-DOS. Turning to the binary compounds, the VB is now divided into two parts corresponding to s-states up to -15 eV in **qtz** BN (-9 eV in **qtz** SiC), followed by a broad block up to EV. The band gap in **qtz** BN is the largest, ~5 eV, which is close to c-BN, while **qtz** SiC has the smallest band gap of about 1.5 eV.

With Pauling electronegativities $\chi B = 2.04$; $\chi C = 2.55$; $\chi N = 3.04$, and $\chi Si = 1.80$, one obtains $\Delta\chi|B\text{-}N| = 1$ and $\Delta\chi|Si\text{-}C| = 0.75$. These results indicate a larger covalence of SiC compared to the polar covalence of BN, hence the larger band gap in boron nitride.

Conclusions

This paper presents a new class of binary compounds with quartz topology using boron nitride and silicon carbide as examples. The structures of **qtz** BN and **qtz** SiC have been constructed from the template carbon allotrope C_6 with quartz topology. It has been shown that the new phases are the densest among all known BN and SiC polymorphs. Accordingly, they are characterized by the highest hardness. In addition to mechanical stability, the new phases are also dynamically stable as indicated by the phonon band structures. The heat capacities of the new phases calculated from the phonon frequencies were found to be higher than those of the corresponding cubic phases; this is also true for **qtz** C_6 compared to diamond. It can be assumed that all of the above is a consequence of the presence of distorted tetrahedra in the crystal structures of the phases with quartz topology. Finally, from the analysis of electronic band structures and densities of states, it was found that the new phases exhibit semiconducting behavior.

Author Contributions: Conceptualization, S.F.M.; methodology, S.F.M. and V.L.S.; investigation, S.F.M. and V.L.S.; formal analysis, S.F.M. and V.L.S.; data curation, S.F.M. and V.L.S.; visualization, S.F.M. and V.L.S.; validation, S.F.M. and V.L.S.; resources, S.F.M.; writing – original draft preparation, S.F.M.; writing – review and editing, V.L.S. Both authors have read and agreed to the published version of the manuscript.

Funding: This research received no external funding.

Data Availability Statement: The data presented in this study are available on reasonable request.

Conflicts of Interest: The authors declare no conflict of interest.

References

[1] Brazhkin, V.V.; Solozhenko, V.L. Myths about new ultrahard phases: Why materials that are significantly superior to diamond in elastic moduli and hardness are impossible. *J. Appl. Phys.* **2019**, *125*, 130901.

[2] Stishov, S.M. Energy, compressibility and covalency in the carbon subgroup. *Philos. Mag. Lett.* 2000, *80*, 125-128.

[3] Qingkun, L.; Yi, S.; Zhiyuan, L.; Yu, Z. Lonsdaleite – A material stronger and stiffer than diamond than diamond. *Scr. Mater.* **2011**, *65*, 229-232.

[4] Öhrström, L.; O'Keeffe, M. Network topology approach to new allotropes of the group 14 elements. *Z. Kristallogr*. **2013**, *228,* 343-346.

[5] Shevchenko, A.P.; Shabalin, A.A.; Karpukhin, I.Yu.; Blatov, V.A. Topological representations of crystal structures: generation, analysis and implementation in the *TopCryst* system. *Sci Technol Adv Mat.* **2022**, *2*, 250-265.

[6] Hoffmann, R.; Kabanov, A.A.; Golov, A.A.; Proserpio, D.M. Homo Citans and carbon allotropes: For an ethics of citation. *Angew. Chem. Int. Ed.* **2016**, *55*, 10962-10976; Samara Carbon Allotrope Database (http://sacada.sctms.ru)

[7] Zhu, Q.; Oganov, A.R.; Salvadó, M.A.; Pertierra, P.; Lyakhov, A.O. Denser than diamond: *Ab initio* search for superdense carbon allotropes. *Phys. Rev. B* **2011**, *83*, 193410.

[8] Luo, B.; Wu, L.; Zhang, Z.; Li, G.; Tian, E. A triatomic carbon and derived pentacarbides with superstrong mechanical properties. *iScience* **2022**, *25*, 104712.

[9] Matar, S.F.; Solozhenko, V.L. First principles search for novel ultrahard high-density carbon allotropes: hexagonal C_6, C_9 and C_{12}. *J. Superhard Mater.* **2023**, *45*, 239-248.

[10] McMahon, M.I.; Nelmes, R.J.; Wright, N.G.; Allan, D.R. Crystal structure studies of II-VI semiconductors using angle-dispersive diffraction techniques with an image-plate detector. *AIP Conf. Proc.* **1994**, *309*, 633-636.

[11] Hohenberg, P.; Kohn, W. Inhomogeneous electron gas. *Phys. Rev. B* **1964**, *136*, 864-871.

[12] Kohn, W.; Sham, L. Self-consistent equations including exchange and correlation effects. *Phys. Rev. A* **1965**, *140*, 1133-1138.

[13] Kresse, G.; Furthmüller, J. Efficient iterative schemes for ab initio total-energy calculations using a plane-wave basis set. *Phys. Rev. B* **1996**, *54*, 11169.

[14] Kresse, G.; Joubert, J. From ultrasoft pseudopotentials to the projector augmented wave. *Phys. Rev. B* **1999**, *59*, 1758-1775.

[15] Blöchl, P.E. Projector augmented wave method. *Phys. Rev. B* **1994**, *50*, 17953-17979.

[16] Perdew, J.; Burke, K.; Ernzerhof, M. The Generalized Gradient Approximation made simple. *Phys. Rev. Lett.* **1996**, *77*, 3865-3868.

[17] Press, W.H.; Flannery, B.P.; Teukolsky, S.A.; Vetterling, W.T. Numerical Recipes, 2nd ed.; Cambridge University Press: New York, USA, 1986.

[18] Blöchl, P.; Jepsen, O.; Anderson, O. Improved tetrahedron method for Brillouin-zone integrations. *Phys. Rev. B* **1994**, *49*, 16223-16233.

[19] Methfessel, M.; Paxton, A. High-precision sampling for Brillouin-zone integration in metals. *Phys. Rev. B* **1989**, *40*, 3616–3621.

[20] Monkhorst, H.; Pack, J. Special k-points for Brillouin Zone integration. *Phys. Rev. B* **1976**, *13*, 5188–5192.

[21] Voigt, W. Über die Beziehung zwischen den beiden Elasticitätsconstanten isotroper Körper. *Annal. Phys.* **1889**, *274*, 573-587.

[22] Blaschke, D.N. Averaging of elastic constants for polycrystals. *J. Appl. Phys.* **2017**, *122*, 145110.

[23] Togo, A.; Tanaka, I. First principles phonon calculations in materials science, *Scr. Mater.* **2015**, *108*, 1-5.

[24] Momma, K.; Izumi, F. VESTA3 for three-dimensional visualization of crystal, volumetric and morphology data. *J. Appl. Crystallogr.* **2011**, *44*, 1272-1276.

[25] Eyert, V. Basic notions and applications of the augmented spherical wave method. *Int. J. Quantum Chem.* **2000**, *77*, 1007-1031.

[26] Mukhanov, V.A.; Kurakevych, O.O.; Solozhenko, V.L. The interrelation between hardness and compressibility of substances and their structure and thermodynamic properties. *J. Superhard Mater.* **2008**, *30*, 368-378.

[27] Lyakhov, A.O.; Oganov, A.R. Evolutionary search for superhard materials: Methodology and applications to forms of carbon and TiO_2. *Phys. Rev. B* **2011**, *84*, 092103.

[28] Mazhnik, E.; Oganov, A.R. A model of hardness and fracture toughness of solids. *J. Appl. Phys.* **2019**, *126*, 125109.

[29] Chen, X-Q.; Niu, H.; Li, D.; Li, Y. Modeling hardness of polycrystalline materials and bulk metallic glasses. *Intermetallics*, **2011**, *19*, 1275-1281.

[30] Solozhenko, V.L.; Matar, S.F. Prediction of novel ultrahard phases in the B–C–N system from first principles: Progress and problems. *Materials* **2023**, *16*, 886.

[31] Bindzus, N.; Straasø, T.; Wahlberg, N.; Becker, J.; Bjerg, L.; Lock, N.; Dippel, A.-C.; Iversen, B.B. Experimental determination of core electron deformation in diamond. *Acta Cryst. A* **2014**, *70*, 39-48.

[32] Ownby, P.D.; Yang, X.; Liu, J. Calculated X-ray diffraction data for diamond polytypes. *J. Am. Ceram. Soc.* **1992**, *75*, 1876-1883.

[33] Solozhenko, V.L.; Chernyshev, V.V.; Fetisov, G.V.; Rybakov, V.B.; Petrusha, I.A. Structure analysis of the cubic boron nitride crystals. *J. Phys. Chem. Solids* **1990**, *51*, 1011-1012.

[34] Zhang, J.S.; Bass, J.D.; Taniguchi, T.; Goncharov, A.F.; Chang, Y.-Y.; Jacobsen, S.D. Elasticity of cubic boron nitride under ambient conditions. *J. Appl. Phys.* **2011**, *109*, 063521.

[35] Kurdyumov, A.V.; Solozhenko, V.L.; Zelyavski, W.B. Lattice parameters of boron nitride polymorphous modifications as a function of their crystal-structure perfection. *J. Appl. Crystallogr*. **1995**, *28*, 540-545.

[36] Solozhenko, V.L.; Häusermann, D.; Mezouar, M.; Kunz, M. Equation of state of wurtzitic boron nitride to 66 GPa. *Appl. Phys. Lett.* **1998**, *72*, 1691-1693.

[37] Li, Z.; Bradt, R.C. Thermal expansion of the cubic (3C) polytype of SiC. *J. Mater. Sci.* **1986**, *21*, 4366-4368.

[38] Lambrecht, W.R.L.; Segall, B., Methfessel, M.; van Schilfgaarde, M. Calculated elastic constants and deformation potentials of cubic SiC. *Phys. Rev. B* **1991**, *44*, 3685-3694.

[39] Krishnan, R.S. Raman spectrum of diamond. *Nature* **1945**, *155*, 171.

[40] Dove, M.T. Introduction to lattice dynamics. Cambridge University Press: New York, USA, 1993.

[41] DeSorbo, W. Specific heat of diamond at low temperatures. *J. Chem. Phys.* **1953**, *21*, 876-880.

[42] Victor, A.C. Heat capacity of diamond at high temperatures. *J. Chem. Phys.* **1962**, *36*, 1903-1911.

[43] Solozhenko, V.L.; Gavrichev, K.S. Thermodynamic properties of boron nitride. in: "*Wide Band Gap Electronic Materials*". (eds. M.A. Prelas et al.), Kluwer Academic Publishers: Dordrecht, Netherlands, 1995, pp. 377-392.

[44] Thermodynamic properties of individual substances (Eds. V.P. Glushko, L.V. Gurvich, G.A. Bergman). Nauka: Moscow, vol. 2, 1978 (in Russian)

Table 1 Crystal structure parameters of phases with quartz topology.

$P6_422$ (No. 181)	C_6 ($C1_3C2_3$)	**qtz** BN	**qtz** SiC
a, Å	2.598	2.595	3.079
c, Å	5.586	5.799	7.054
V_{cell}, Å^3	32.65	33.83	57.90
$<V_{atom}>$ Å^3	5.44	5.64	9.65
Shortest bond, Å	1.598	1.64	1.936
Angles (deg.)	108.73 / 90.52	106.64 / 92.0	105.26 / 93.01
Atomic positions	C1 (3c) ½, 0, 0 C2 (3d) ½, 0, ½	B (3c) ½, 0, 0 N (3d) ½, 0, ½	Si (3c) ½, 0, 0 C (3d) ½, 0, ½
E_{total}, eV E_{coh}/atom, eV	-47.87 -1.38	-46.65 -1.73	-41.79 -1.15

Table 2 Elastic constants (C_{ij}) of phases with quartz topology. Bulk (B_V) and shear (G_V) moduli calculated by the Voight averaging. All values are in GPa.

	C_{11}	C_{12}	C_{13}	C_{33}	C_{44}	C_{66}	B_V	G_V
qtz C_6 [9]	1184	88	63	1161	548	539	440	546
qtz BN	892	164	109	1013	364	342	396	370
qtz SiC	448	87	97	598	180	201	228	197

Table 3 Vickers hardness (H_V) and bulk moduli (B_0) of dense carbon, BN and SiC phases calculated using the thermodynamic model of hardness [26]

	Space group	$a = b$ (Å)	c (Å)	ρ (g/cm^3)	H_V (GPa)	B_0 (GPa)
Diamond	*Fd*-3*m*	3.56661 [31]		3.517	98	445 [1]
Lonsdaleite	$P6_3/mmc$	2.5221 [32]	4.1186 [32]	3.516	97	443
qtz C_3 #180 [7]	$P6_222$	2.605 [7]	2.801 [7]	3.635	101	460
qtz C_3 #180 [8]	$P6_222$	2.613 [8]	2.811 [8]	3.600	100	456
qtz C_6 #181	$P6_222$	2.5970	5.5865	3.667	102	464
c-BN #216	*F*-43*m*	3.6160 [33]		3.487	55	381 [34]
w-BN #186	$P6_3mc$	2.5505 [35]	4.210 [35]	3.475	54	375 [36]
qtz BN #181	$P6_422$	2.5954	5.7993	3.654	58	395
SiC (3C) #216	*F*-43*m*	4.3581 [37]		3.218	34	238
qtz SiC #180	$P6_222$	3.0787	7.0537	3.450	36	255

Table 4 Mechanical properties of dense carbon, BN and SiC phases: Vickers hardness (H_V), bulk modulus (B), shear modulus (G), Young's modulus (E), Poisson's ratio (ν) and fracture toughness (K_{Ic})

	H_V				B		G_V	E[**]	ν[**]	K_{Ic}[‡]
	T[*]	LO[†]	MO[‡]	CN[§]	B_0[*]	B_V				
	GPa									MPa·m^{½}
Diamond	98	90	100	93	445 [1]		530 [1]	1138	0.074	6.4
Lonsdaleite	97	90	99	94	443	432	521	1115	0.070	6.2
qtz C_3 [#180] [7]	101	90	–	88 [7]	460	433 [7]	–	–	–	–
qtz C_3 [#180] [8]	100	88	113 [8]	110	456	452 [8]	587 [8]	1229	0.047	6.8
qtz C_6 [#181]	102	90	104	100	464	440	546	1159	0.061	6.4
c-BN [#216]	55	50	73	67	381 [34]		399 [34]	887	0.112	4.8
w-BN [#186]	54	50	72	65	375 [36]	390	397	889	0.120	5.1
qtz BN [#181]	58	51	63	56	395	396	370	847	0.143	6.4
SiC (3C) [#216]	34	30	32	35	238	225[††]	199[††]	461[††]	0.153[††]	3.3
qtz SiC [#180]	36	31	31	34	255	228	197	460	0.165	3.3

[*] Ref. 26

[†] Ref. 27

[‡] Ref. 28

[§] Ref. 29

[**] E and ν values calculated using isotropic approximation

[††] Calculated by Voigt averaging of literature data on elastic constants [38]

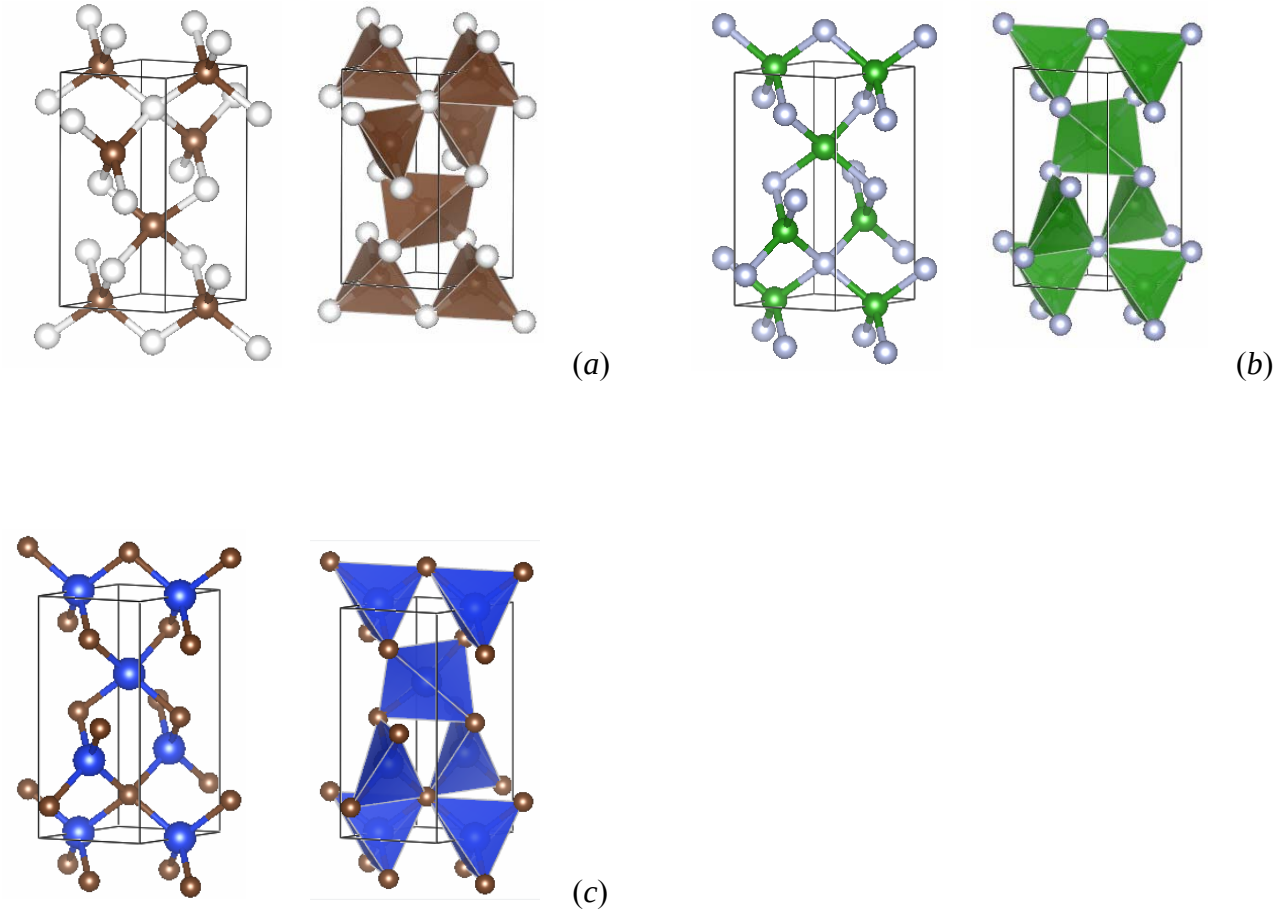

Figure 1. Ball-and-stick and tetrahedral representations of the crystal structures of three phases with quartz topology: (*a*) C_6 or $C1_3C2_3$ (cf. Table 1) (brown and white balls for C1 and C2, respectively), (*b*) BN (green and gray balls for B and N), (*c*) SiC (blue and brown balls for Si and C).

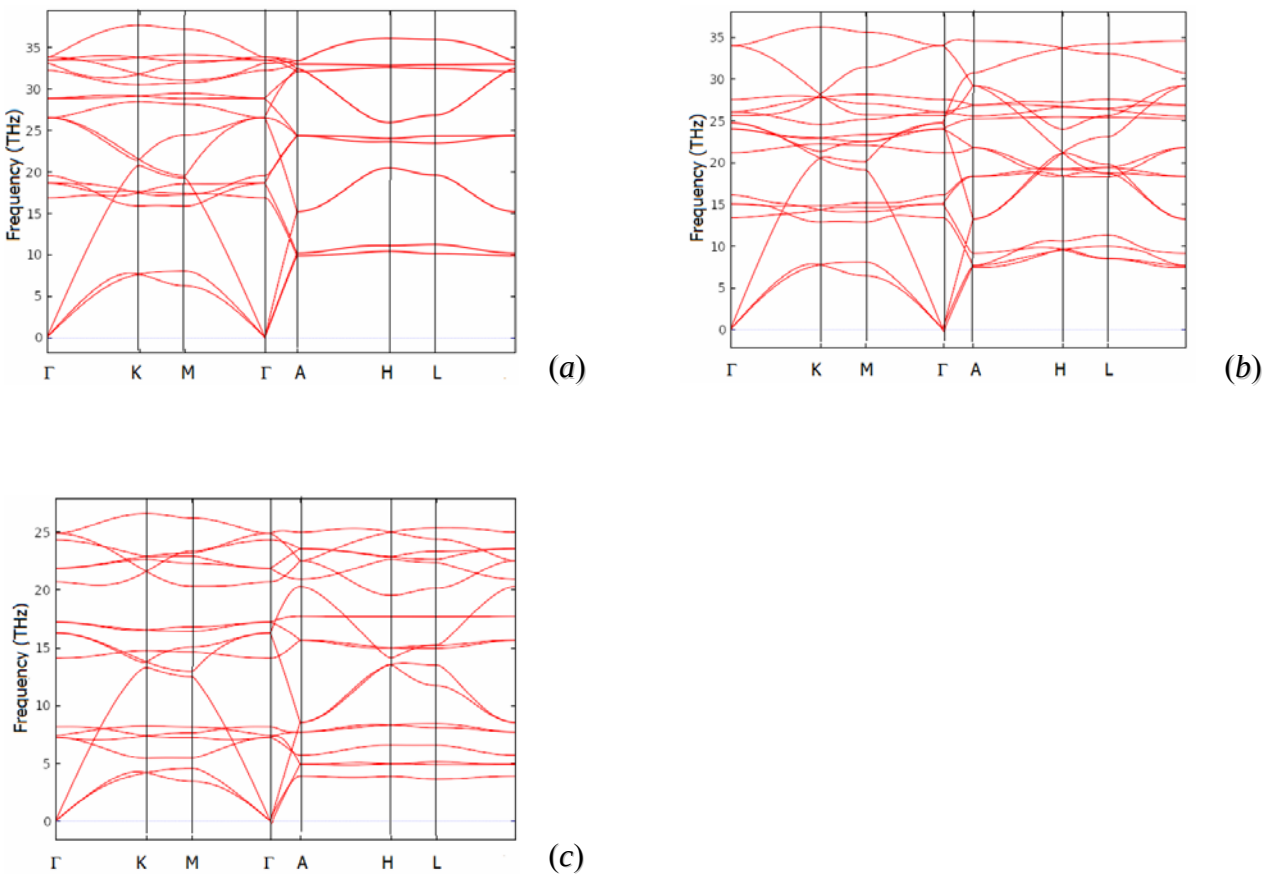

Figure 2. Phonons band structures of **qtz** C_6 (*a*), **qtz** BN (*b*) and **qtz** SiC (*c*).

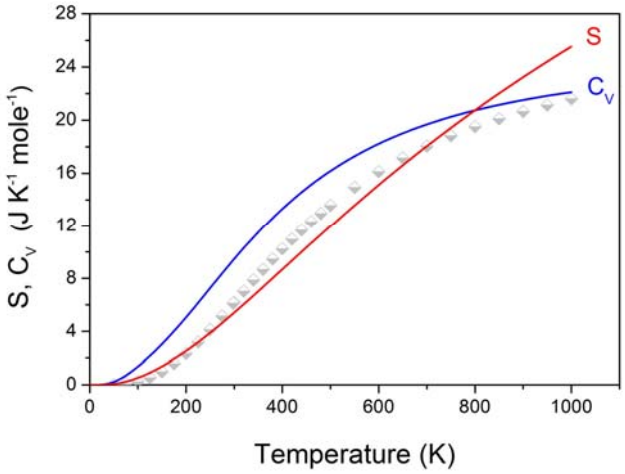

(*a*)

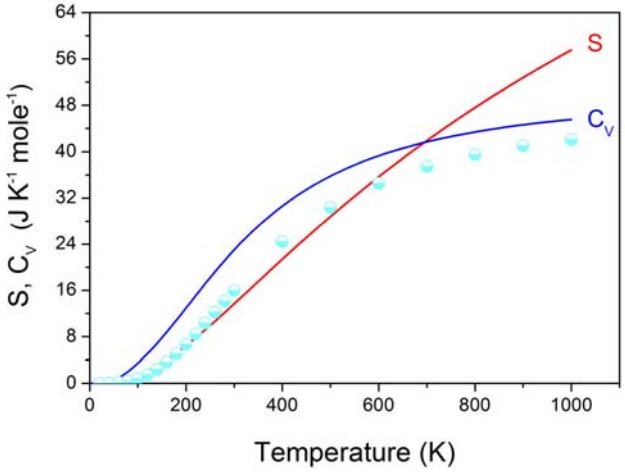

(*b*)

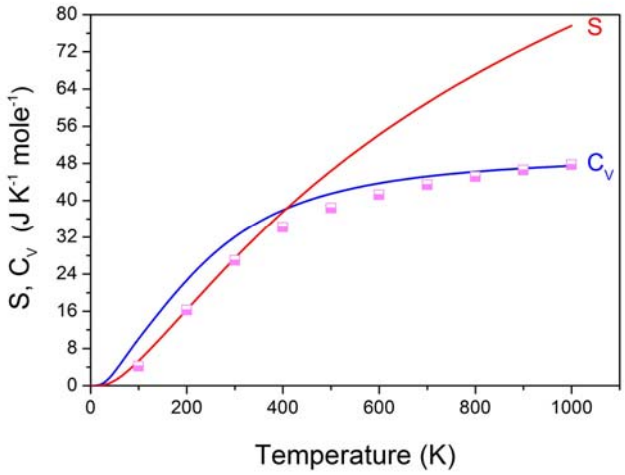

(*c*)

Figure 3. Heat capacity at constant volume and entropy of **qtz** C_6 (*a*), **qtz** BN (*b*) and **qtz** SiC (*c*) as functions of temperature. Experimental heat capacity data for diamond [41,42], cubic BN [43] and cubic SiC [44] are shown as gray, cyan and magenta symbols, respectively.

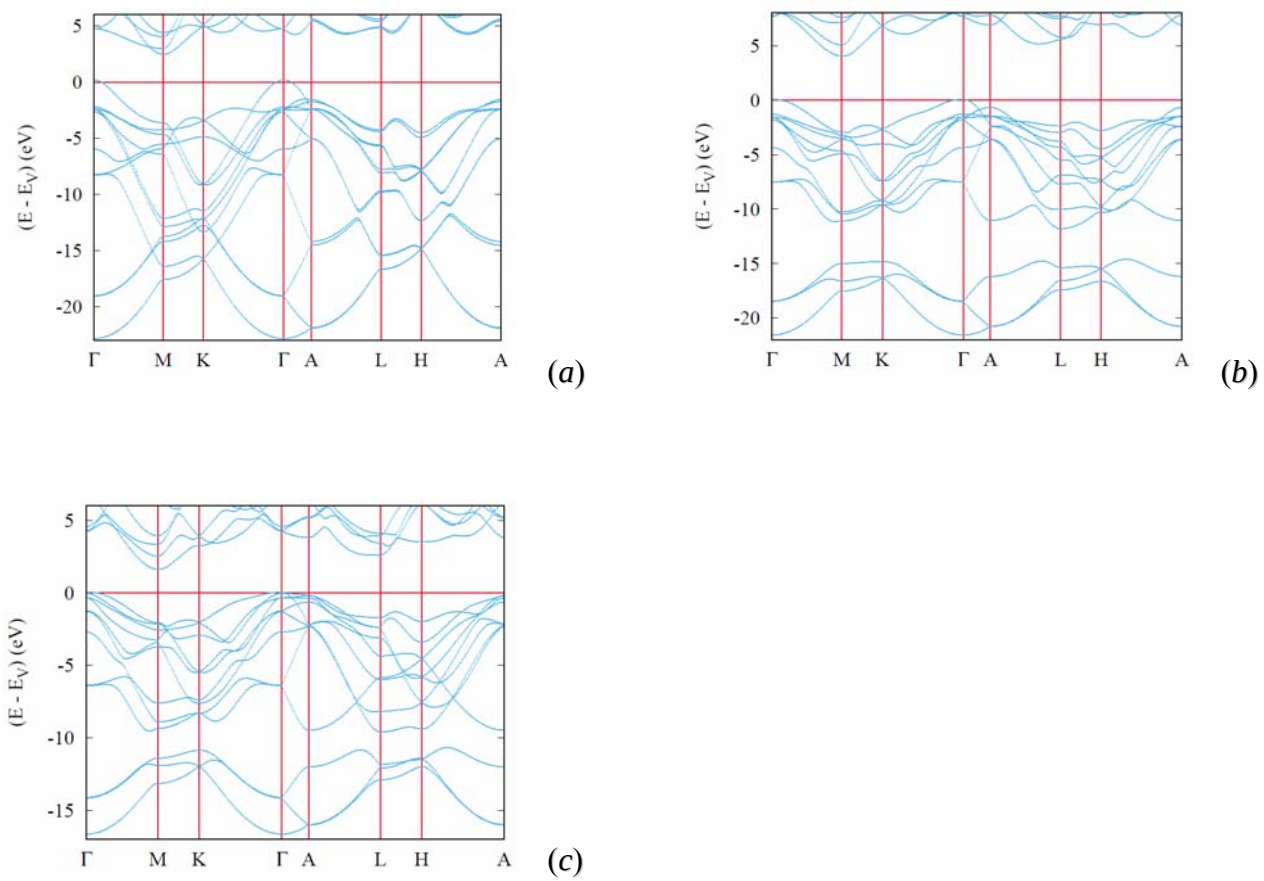

Figure 4. Electronic band structures of **qtz** C_6 (*a*), **qtz** BN (*b*) and **qtz** SiC (*c*).

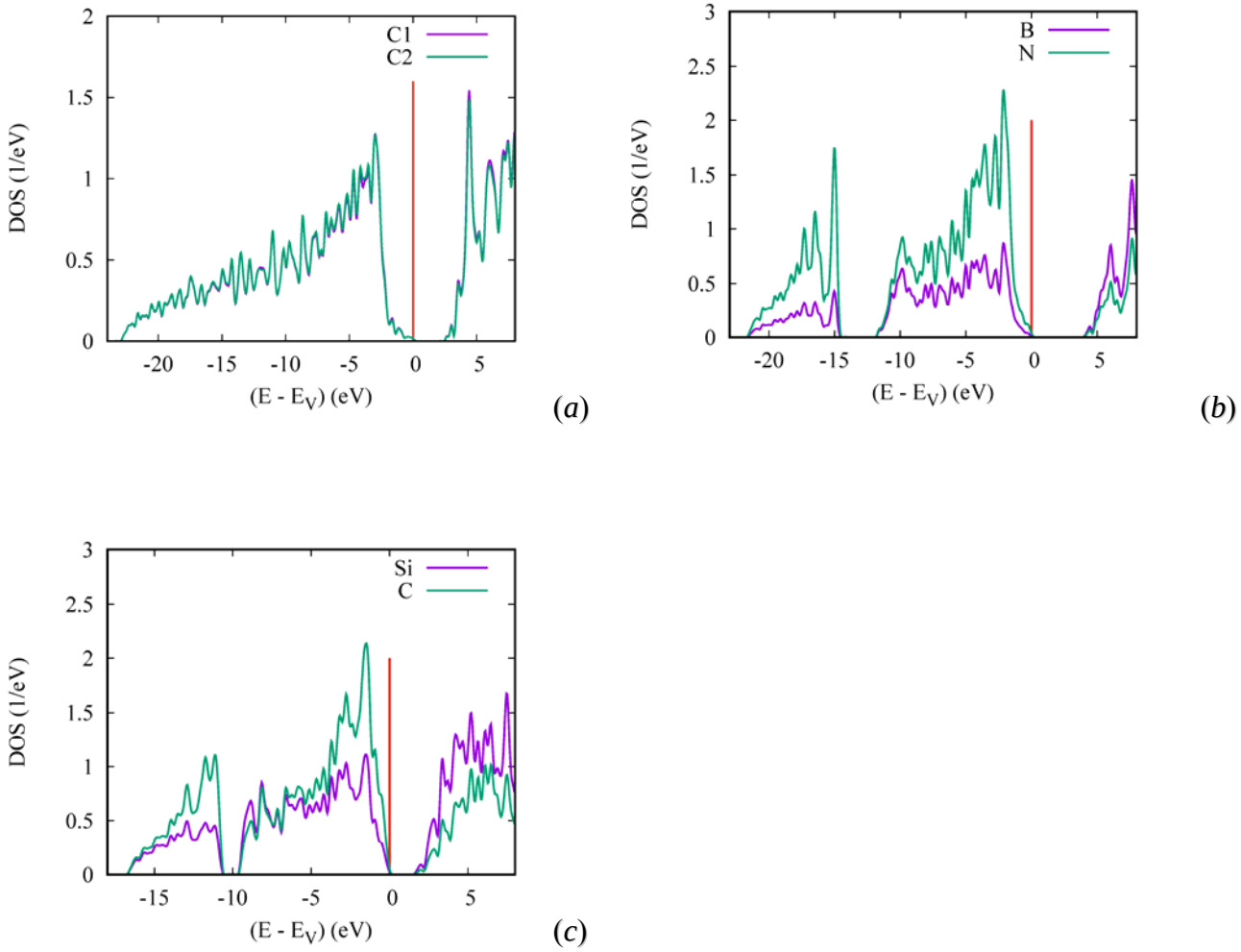

Figure 5. Site projected density of states of **qtz** C_6 (*a*), **qtz** BN (*b*) and **qtz** SiC (*c*).